Biologically Representative Lipid-Coated Gold Nanoparticles and Phospholipid Vesicles for the Study of Alpha-Synuclein/Membrane Interactions

Sophia M. McClain^a, Moses H. Milchberg^b, Chad M. Rienstra^{bc}, Catherine J. Murphy^a*

^aDepartment of Chemistry, University of Illinois Urbana-Champaign, 600 South Mathews Avenue, Urbana, Illinois, USA;

^bDepartment of Biochemistry, University of Wisconsin-Madison, 433 Babcock Drive, Madison, Wisconsin, USA;

^cNational Magnetic Resonance Facility at Madison, University of Wisconsin-Madison, 433 Babcock Drive, Madison, Wisconsin, USA

*C.J.M. Email: murphycj@illinois.edu

ABSTRACT Alpha-synuclein is an intrinsically disordered protein whose formation of beta-sheet rich protein aggregates in the brain is implicated in the development of Parkinson's disease. Due to its believed role in synaptic vesicle trafficking and neurotransmission, many studies have employed simple, synthetic model systems to investigate alpha-synuclein/membrane interactions in an attempt to gain a better understanding of the protein's native and pathogenic functions. Interestingly, these studies seem to suggest that alpha-synuclein interacts differently with rigid vesicle mimics in comparison to malleable vesicle mimics. However, the use of different mimic sizes and surface chemistries across existing studies makes it challenging to directly compare the effects of membrane mechanical properties on protein behavior observed thus far. In this work, we

developed a synaptic vesicle mimic library comprising a range of both malleable and rigid synaptic vesicle mimics possessing the same size and biologically representative lipid surface chemistry. Limited proteolysis mass spectrometry experiments revealed distinct fragmentation patterns between rigid and malleable synaptic vesicle mimics. The N-terminal and C-terminal regions of alpha-synuclein were found to become less solvent-accessible upon binding to all synaptic vesicle mimics. Nevertheless, minor variations in digestion pattern were observed in the central region of the protein dependent upon mimic size, rigidity, and lipid composition. Higher binding affinities were observed for alpha-synuclein binding to rigid synaptic vesicle mimics compared to malleable synaptic vesicle mimics. Additionally, the binding affinity of alpha-synuclein toward small lipid vesicles and small lipid-coated gold nanoparticles without cholesterol was found to be lower than their respective malleable and rigid counterparts. Interestingly, the binding curves for the rigid synaptic vesicle mimics demonstrated a non-traditional peak and dip shape believed to arise from differences in alpha-synuclein orientation on the particle surface at different protein-to-particle incubation ratios.

KEYWORDS alpha-synuclein, synaptic vesicle mimics, phospholipids, cholesterol, gold nanoparticles, limited proteolysis

Abnormal misfolding and aggregation of alpha-synuclein, a naturally abundant neuronal protein, has been implicated in the development of several neurodegenerative diseases, including Parkinson's disease, due to its incorporation as the major component of Lewy bodies and Lewy neurites which represent a pathological hallmark of these conditions. While alpha-synuclein is considered an intrinsically disordered protein in its unbound monomeric state, 4 it adopts distinct secondary structure characteristics associated with both its native and disease states providing a convenient handle for monitoring protein behavior. Pathogenic fibrillation of alpha-synuclein is

marked by an increase in beta-sheet structure propagating from the central, hydrophobic region of the protein known as the NAC or non-amyloid beta component.^{5–8} On the other hand, an increase in alpha-helix structure is observed upon binding of alpha-synuclein to anionic membranes facilitated by an imperfect series of repeating amphipathic motifs located in the N-terminal region of the protein.^{9–12} Membrane binding is also an important aspect of alpha-synuclein's proposed biological function in the regulation of synaptic activities including docking of synaptic vesicles, endocytosis, synaptic vesicle clustering, and membrane remodeling.^{13–16} Significantly, six alpha-synuclein point mutations currently known to be associated with the development of hereditary Parkinson's disease are located within the N-terminal binding region.^{17,18} These mutants have been shown to impact both lipid binding behavior and alpha-synuclein aggregation kinetics.¹⁸ Taken together, these observations suggest that modulation of alpha-synuclein's membrane binding abilities could play an important role in disease pathology.

As a result, researchers have investigated the interactions of alpha-synuclein with a variety of model membrane surfaces in an attempt to gain a better understanding of the protein's native function and its role in disease states. These studies have shown that alpha-synuclein binds to highly curved surfaces such as small detergent micelles *via* a broken helical structure, while binding to larger vesicles with less curved surfaces *via* an extended helical structure. Factors including vesicle size, membrane composition, and alpha-synuclein point mutation have also been observed to influence protein binding strength. Typically, alpha-synuclein exhibits stronger binding to small vesicles in comparison to large vesicles, 9,21,22 as well as a greater affinity for anionic membranes in comparison to neutral membranes. Furthermore, the A30P variant of alpha-synuclein exhibits decreased binding in comparison to wild-type alpha-synuclein, while the E46K variant exhibits increased binding. R2,21,24,25 Interestingly, for a series of rigid lipid vesicle

mimics comprising spherical gold nanoparticles coated with a sodium dodecyl sulfate-based organic bilayer, we observed no significant trends in binding affinity related to either alphasynuclein variant or particle size. This suggests that the native malleability of lipid vesicles could play an important role in modulating the binding behaviors of alpha-synuclein. However, the use of varied surface chemistries, mimic sizes, and experimental conditions across studies has made it difficult to directly compare existing data to assess the effects of membrane mechanical properties on protein behavior.

In this study we developed a library comprising both malleable (lipid vesicle) and rigid (lipidcoated gold nanoparticle) synaptic vesicle mimics possessing the same hydrodynamic diameter and surface chemistry to facilitate a systematic investigation into the impact of membrane mechanical properties on alpha-synuclein binding interactions. By using a mixture of phospholipids representative of those most prevalently found in synaptic vesicles, ^{27,28} we were able to better approximate biological complexity while also achieving size control over malleable synaptic vesicle mimics which would not have been possible with our previous sodium dodecyl sulfate-based system.²⁶ Furthermore, incorporation of 0-20 mol% cholesterol into both the malleable lipid vesicles and rigid lipid-coated gold nanoparticles provided our system with additional moderate variations in mimic malleability as well as two distinct surface chemistries for comparison. Significantly, epidemiological studies have implicated cholesterol dysregulation in the pathogenesis of neurodegenerative diseases, 29,30 while various in vitro experiments have demonstrated that varying the amount of cholesterol present in synthetic vesicles affects both the binding affinity of alpha-synuclein for the vesicles^{31,32} and the protein's ability to deform the vesicles from spheres into tubules.³³ Here we used dynamic light scattering, circular dichroism,

and mass spectrometry approaches to probe properties including binding affinity and protein orientation upon interaction between alpha-synuclein and our library of synaptic vesicle mimics.

RESULTS AND DISCUSSION

Synthesis and Characterization of Biologically Representative Mimic Library. A library of synaptic vesicle mimics with varying degrees of deformability ranging from malleable phospholipid vesicles to rigid lipid-coated gold nanoparticles were synthesized (Figure 1). A set of "small" mimics within the biological size range²⁷ of ~40-80 nm and a set of "large" mimics (>100 nm) were prepared using a biologically representative combination of lipids with a molar ratio of DOPC(3):DOPE(3):DOPS(1):SM(1) which approximates the reported composition of synaptic vesicles.²⁸ Incorporation of cholesterol into this lipid composition to achieve a molar ratio of DOPC(3):DOPE(3):DOPS(1):SM(1):Chol(2) and further addition of a gold nanoparticle core afforded varying degrees of rigidity to the mimics.

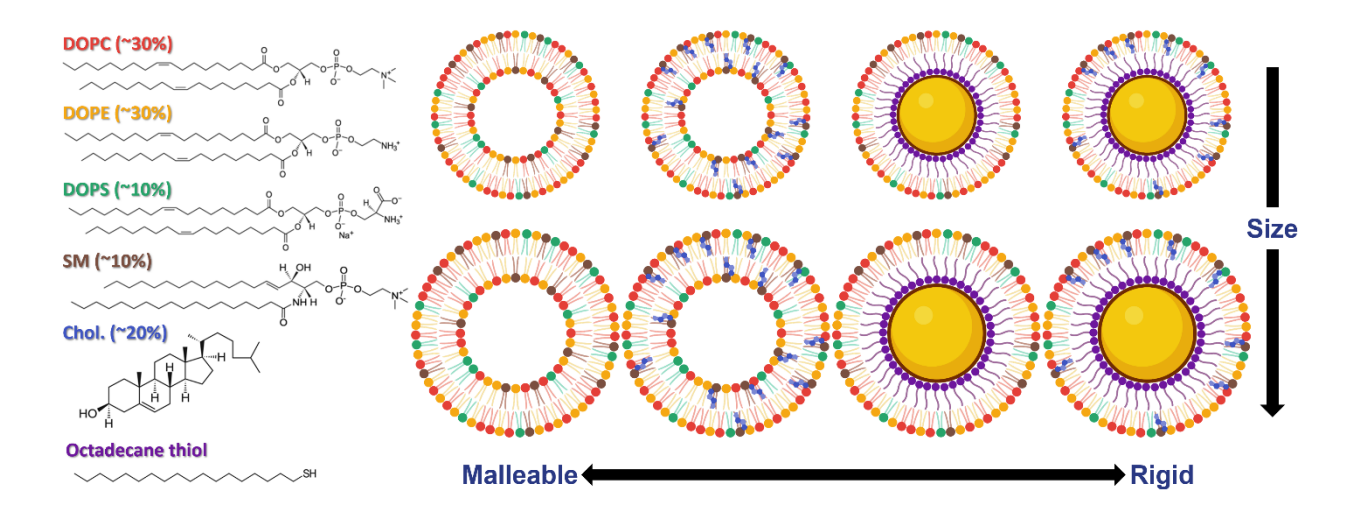


Figure 1. Library of synaptic vesicle mimics with varying degrees of deformability ranging from malleable phospholipid vesicles to rigid lipid-coated gold nanoparticles. Lipids employed in the synthesis of these mimics include DOPC (red), DOPE (yellow), DOPS (green), sphingomyelin (brown), and cholesterol (blue). The given percentages represent the molar ratio of lipids used in mimic synthesis. An inner layer of octadecane thiol (purple) anchors an outer layer containing the lipids of interest to the surface of gold nanoparticle-based mimics. Illustrations of synaptic vesicle mimics created using BioRender.

First, citrate-capped gold nanoparticles were synthesized in the two desired size regimes and characterized by transmission electron microscopy to have core diameters of approximately 50 and 120 nm for small and large particles respectively (Figures S1-S2). Lipid-coating of these citrate-capped gold nanoparticles resulted in a 5-8 nm redshift of the particles' extinction peak (Figure 2A) which is indicative of an increase in refractive index at the particles' surface due to a change in surface chemistry. Additionally, a ~10 nm increase in the hydrodynamic diameter (Figure 2B) of the particles upon lipid-coating is in good agreement with the estimated 4 nm thickness34,35 of the desired organic bilayer. Small, coated particles possessed a final hydrodynamic diameter of approximately 70-75 nm while large, coated particles possessed a final hydrodynamic diameter of approximately 120-130 nm, both in good agreement with the hydrodynamic sizes of small and large extruded vesicles (Figure 2B, Figure S3). It was observed, particularly for malleable synaptic vesicle mimics, that lipid compositions containing cholesterol typically resulted in mimics with a slightly larger hydrodynamic diameter than those not containing cholesterol. This is a commonly observed trend and is likely due to the impact of increased bending modulus afforded by cholesterol incorporation on the mechanics of vesicle extrusion. ^{36,37} Negative zeta potential measurements were obtained for all lipid-coated particles and extruded phospholipid vesicles (Figure 2C, Figure S4). This result is in accordance with the net negative charge of the lipid mixtures used in these experiments wherein DOPC, DOPE, sphingomyelin, and cholesterol are overall neutral molecules, while DOPS possesses an anionic headgroup.

Subsequent etching experiments showed that both small and large lipid-coated gold nanoparticles were highly resistant to etching in the presence of >10 fold excess potassium cyanide. While the original citrate-capped gold nanoparticles were completely etched away in approximately 10-15 minutes, little to no decrease in absorbance was observed over the course of

20 minutes for lipid-coated gold nanoparticles under the same conditions (**Figure 2D**). This observation indicates the successful formation of a compact hybrid lipid coating on the particle surface, which possesses a hydrophobic region capable of preventing permeation by cyanide ions. Protection against cyanide etching was maintained long term, with particles maintaining >90% extinction after 4 months and >50% extinction after 2 years of constant cyanide exposure (**Figure 2E**). Finally, staining of the lipid-coated gold nanoparticles with osmium tetroxide allowed for

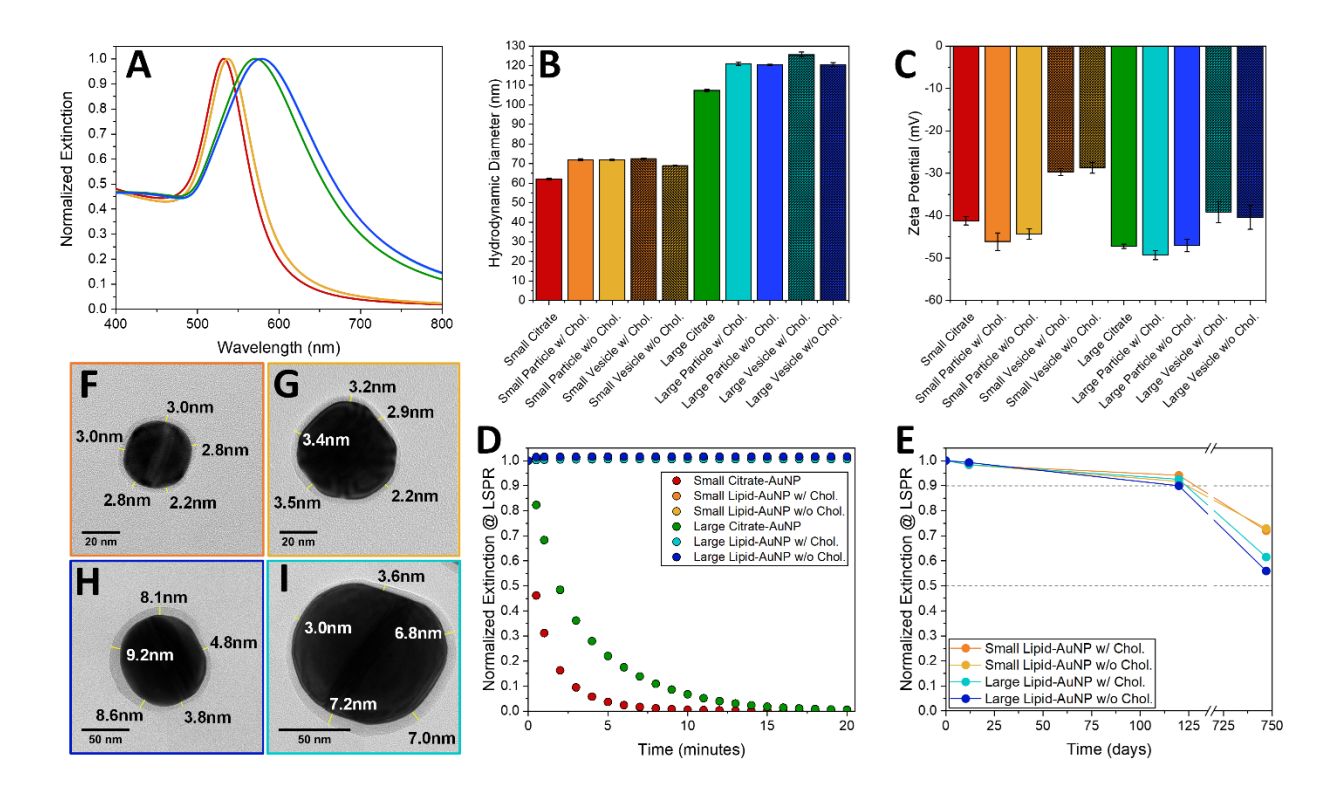


Figure 2. Characterization of representative citrate-capped and lipid-coated gold nanoparticles (solid), as well as extruded phospholipid vesicles (textured). a) UV-vis spectra of small citrate-capped gold nanoparticles (red), small lipid-coated gold nanoparticles with cholesterol (orange), small lipid-coated gold nanoparticles without cholesterol (yellow), large citrate-capped gold nanoparticles (green), large lipid-coated gold nanoparticles with cholesterol (light blue), and large lipid-coated gold nanoparticles without cholesterol (dark blue) gold nanoparticles, b) hydrodynamic diameter of all sample types, c) zeta potential of all sample types, d-e) normalized absorbance of gold nanoparticle-based samples after exposure to excess potassium cyanide, f-i) transmission electron microscopy images of small lipid-coated gold nanoparticles with cholesterol (orange), small lipid-coated gold nanoparticles without cholesterol (yellow), large lipid-coated gold nanoparticles with cholesterol (light blue), large lipid-coated gold nanoparticles without cholesterol (dark blue) stained using osmium tetroxide.

visual confirmation of the lipid coatings by transmission electron microscopy (**Figure 2F-I**, **Figure S5-S6**). By this approach, lipid coatings were observed to have a thickness measuring in the range of $\sim 2-9$ nm. This variation could be a result of drying effects upon sample preparation or an indication of multilayer formation on certain particles.

When synthesizing lipid vesicles comprising a mixture of different lipid components, it is standard practice to assume that the ratio of lipids going into the synthesis is maintained in the final vesicle product. However, when coating nanoparticles with a mixture of different lipid components, it has been observed that some lipids demonstrate preferential adsorption over others to the nanoparticle surface, with additional influences arising from nanoparticle size and coating protocol. 38,39 Furthermore, when vesicles are synthesized by extrusion through a porous membrane, as they were for this study, it is reasonable to believe that some lipids may preferentially interact with and become stuck on the membrane material during synthesis, thereby impacting the ratio of lipids in the final extruded vesicles. Due to these considerations, we wanted to quantify the final composition of lipid components present in all of our synaptic vesicle mimics. This quantification would allow us to determine whether preferential adsorption was taking place during the synthesis of our mimics and confirm that the surface chemistry of all mimics was comparable to enable more meaningful interpretation of results from subsequent interaction studies.

Liquid chromatography-mass spectrometry was used to quantify the amount of DOPC, DOPE, and DOPS present in samples, while cholesterol was quantified using a fluorometric assay. However, the sphingomyelin used in these experiments was obtained as a brain extract containing a mixture of molecular structures, making direct quantification of this component more challenging. Instead, we utilized a mass balance approach to quantify sphingomyelin by

subtracting the measured DOPC, DOPE, and DOPS concentrations from a total phosphorus concentration determined by colorimetric assay or inductively coupled plasma-mass spectrometry analysis (Scheme S1). Unfortunately, this approach produced varied results and lacked reproducibility. While some replicates yielded calculated sphingomyelin concentrations in the expected range, the majority of replicates for all samples as well as the original lipid mixture had aberrantly high apparent sphingomyelin concentrations ranging from 2 to 20 times the amount of sphingomyelin actually added to the original lipid mixture and translating to ~10-75% sphingomyelin in the final lipid composition. Although we cannot conclude much from this attempted quantification of sphingomyelin, quantification of the remaining lipid components was well behaved and reproducible, showing a comparable molar ratio of lipid components present between each malleable synaptic vesicle mimic and its respective original lipid mixture (Figure 3).

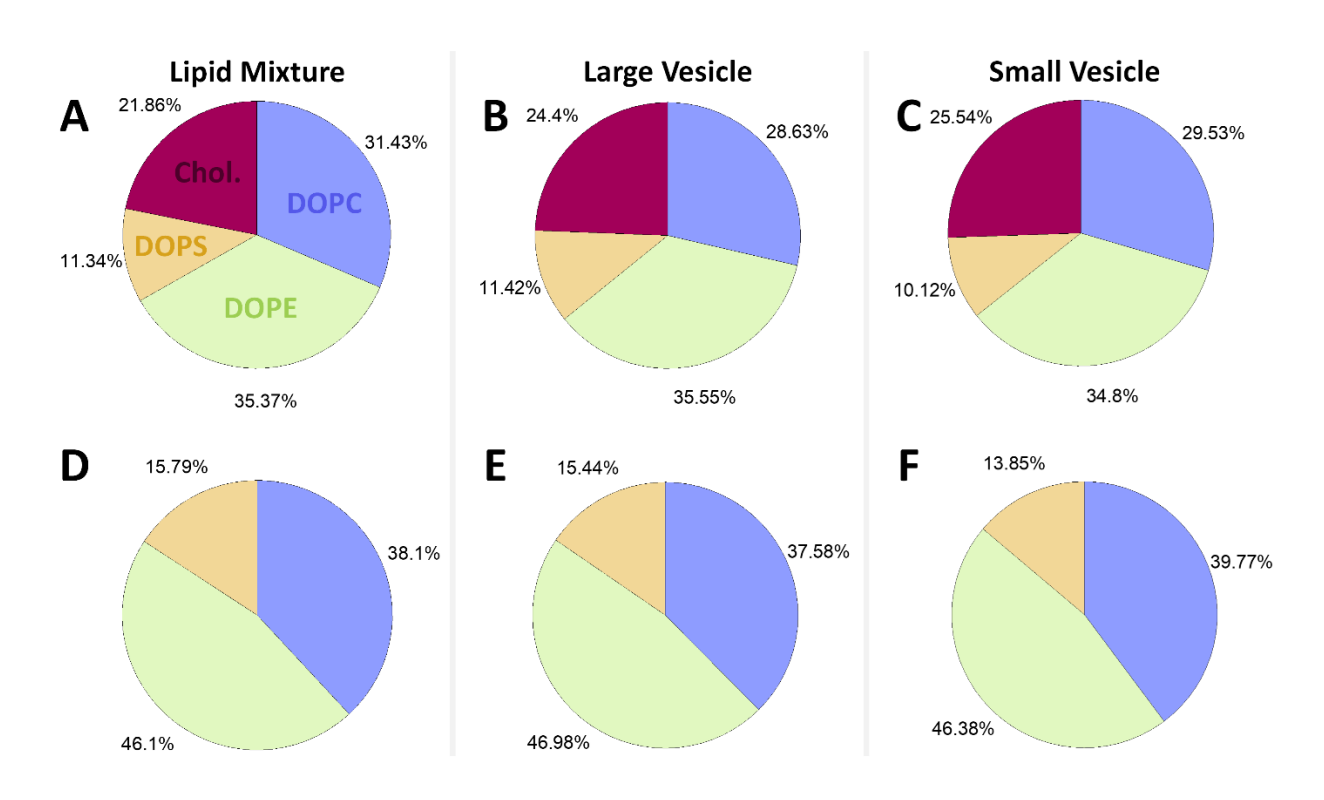


Figure 3. Molar ratio of DOPC (blue), DOPE (green), DOPS (yellow), and cholesterol (purple) measured in large and small extruded phospholipid vesicles as well as the lipid mixtures used in their synthesis. Lipid compositions are given for samples prepared a-c) with cholesterol and d-f) without cholesterol.

For the quantification of the lipids coating our rigid synaptic vesicle mimics, the lipids first needed to be extracted from the nanoparticles' surface using an adapted approach to the Folch extraction method. 40,41 Using this approach, relatively equal and efficient extraction of all lipid species was achieved for the lipid mixture alone in the absence of gold nanoparticles (Figure S7A-C). However, extraction efficiency was variable between replicate extractions of lipids from the surface of coated gold nanoparticle samples (Figure S7D-G), particularly for DOPC, DOPE, and DOPS when compared to cholesterol. While some lipid extractions from the particles' surface matched the ratio of lipids used for mimic synthesis (e.g., S7G vs. S7B), this result was not consistently observed. These inconsistent outcomes could be due to actual variations in lipid composition on the particles' surface, however; it could also be the result of incomplete lipid extraction from samples containing gold nanoparticles. Solid-state nuclear magnetic resonance spectroscopy (SSNMR) was investigated as a possible alternative technique by which to quantify lipid composition without the need for extraction from the particles' surface. Unfortunately, differences in relaxation rates and linewidths prevented lipid quantification by this approach as well. Nevertheless, ³¹P-detected SSNMR experiments did provide support for the rigidification of the particles' surface chemistry upon addition of cholesterol (Figure S8). Although several hurdles prevented conclusive analysis of all lipid components, the data obtained seem to suggest that for the lipids and experimental conditions used in this study, the assumption that the ratio of lipids going into mimic synthesis is maintained in the final mimic product generally holds true.

Alpha-Synuclein/Rigid Mimic Binding Affinity by Dynamic Light Scattering Titrations.

Dynamic light scattering was used to monitor the binding affinity between alpha-synuclein and lipid-coated gold nanoparticles. For these experiments, the concentration of lipid-coated gold

nanoparticles was kept constant as the amount of alpha-synuclein added to the particles was increased. With increasing protein concentration, the hydrodynamic diameter of the particles is expected to increase as more and more proteins bind until it plateaus indicating saturation of the particle surface. However, for all replicates of all lipid-coated gold nanoparticle types, an initial increase in hydrodynamic diameter was observed with increasing protein concentration followed by a decrease in hydrodynamic diameter as the protein concentration continued to rise (Figure 4). This breaks from the expected and previously observed outcome of a plateau in hydrodynamic diameter at high protein concentrations²⁶ and warrants further investigation to understand what is causing this behavior. One possible explanation is that past the peak of the titration curve the protein shell begins compressing or disrupting the soft lipid coating on the particle surface leading to the smaller overall hydrodynamic size of the resulting complexes. Previous work investigating alpha-synuclein binding to 1-palmitoyl-2-oleoyl-sn-glycero-3-phospho-L-serine (POPS) vesicles also suggests that increasing protein concentrations could play a role in destabilizing lipid bilavers. 42 In order to test if the lipid coating is being destabilized by alpha-synuclein binding, a full set of titration points were exposed to excess potassium cyanide to assess lipid coating integrity (Figure S9). No etching of the gold nanoparticles was observed at any protein concentration indicating that the gold cores remained protected from cyanide penetration. However, this protection could arise from a compact protein layer coating the exterior of the particles and therefore cannot be interpreted as conclusive evidence relating to the condition of the lipid coating. Interestingly, the peak and dip binding curve shape was observed for both typical titrations in which samples were measured as prepared after incubation and for titrations in which incubated samples were washed once by centrifugation before measurement (Figure S10). This indicates that removal of excess protein does not change the shape of the binding curves. Another potential

explanation for the observed dipping behavior in the binding curves could be a change in alphasynuclein display on the surface of the particles at higher concentrations due to multilayer adsorption or crowding on the particle surface. We will explore this possibility further in our discussion of limited proteolysis mass spectrometry experiments below.

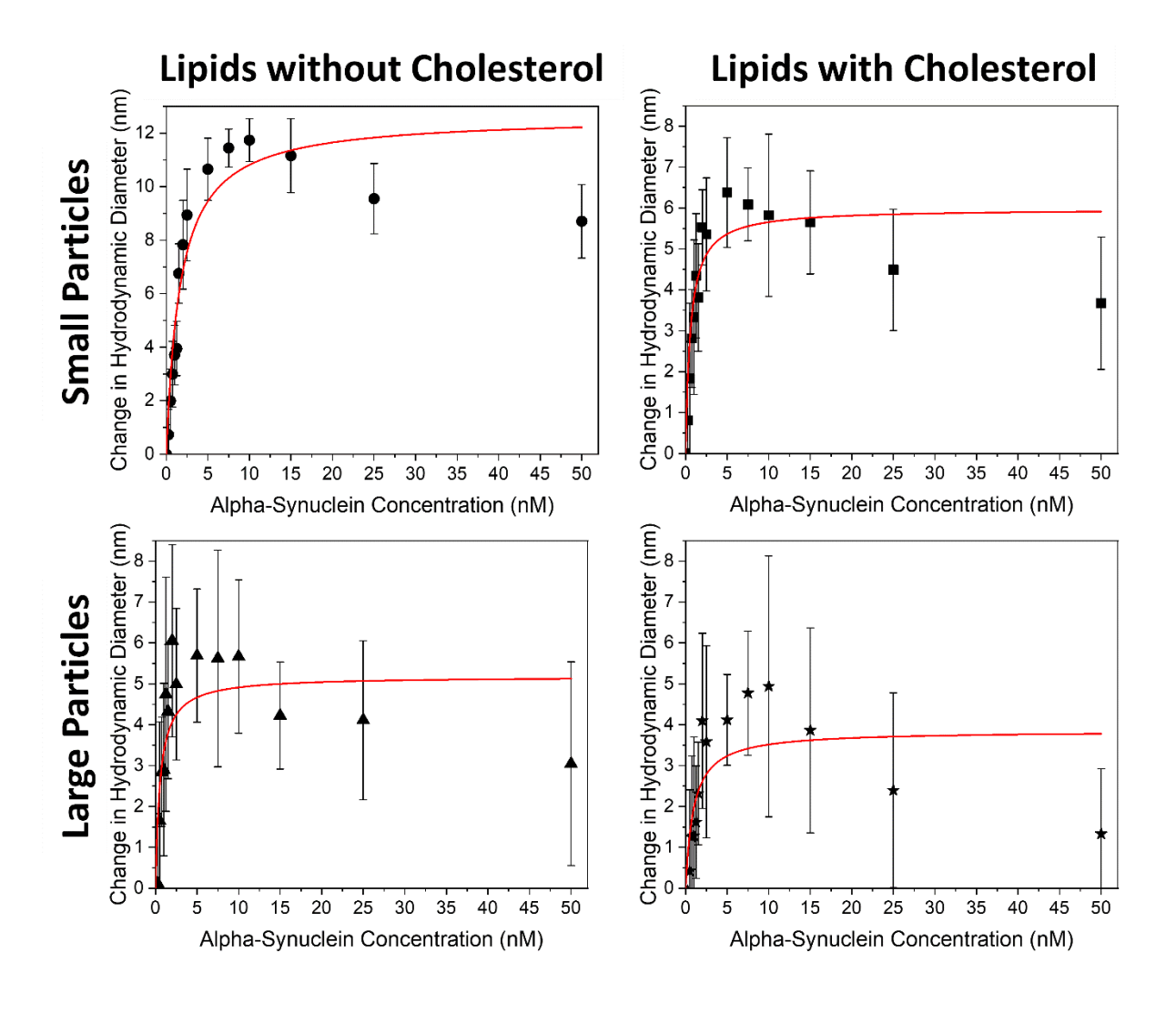


Figure 4. Dynamic light scattering titrations of lipid-coated gold nanoparticles with alpha-synuclein. The change in hydrodynamic diameter of lipid-coated gold nanoparticles is plotted as a function of alpha-synuclein concentration. The data shown here is an average of three replicate titrations for each condition. Error bars represent the standard deviation of the averaged replicates. Fitting of the data with a Langmuir Adsorption Isotherm is shown in red.

Apparent association constants (K_a) for each lipid-coated gold nanoparticle/alpha-synuclein pairing were estimated by fitting their respective binding curves using a Langmuir

Adsorption Isotherm (**Equation 1**) in which ΔD is the change in hydrodynamic diameter at a given titration point, ΔD_{max} is the maximum change in hydrodynamic diameter, and [AS] is the concentration of alpha-synuclein at a given titration point.

$$\frac{\Delta D}{\Delta D_{max}} = \frac{K_a[AS]}{1 + K_a[AS]}$$
 (Equation 1)

Although the peak and dip binding curve shape observed here is not typical of Langmuir-type binding behavior, fitting of the isotherm to real data is primarily influenced by the slope of the initial increase which does behave as expected in this system. Furthermore, replacement of the dip regime with an artificial plateau yields very similar values for the association constants (Figure S11), suggesting this approach can be used with caution to estimate binding constants. Estimated association constants (Table 1) for large lipid-coated gold nanoparticles with and without cholesterol as well as small lipid-coated gold nanoparticles with cholesterol all fell in the range of (1.1-1.8) × 10⁹ M⁻¹. However, small lipid-coated gold nanoparticles without cholesterol yielded a slightly lower association constant of $5.9 \times 10^8 \,\mathrm{M}^{-1}$. Interestingly, the association constants for the current lipid-coated gold nanoparticle mimics are roughly 1-2 orders of magnitude higher than previously studied sodium dodecyl sulfate-coated gold nanoparticles ($K_a = (2.1-5.9) \times 10^7 \text{ M}^{-1}$) analyzed by the same approach. This increased affinity could be a result of packing defects and grain boundaries arising in the more complex, mixed lipid surface chemistry as previous studies have suggested that alpha-synuclein exhibits heightened affinity for such defects in lipid bilayers. 22,44,45 However, factors such as ionic strength, pH, and temperature can also impact protein binding affinities^{46–48} and should be considered as a point of caution when comparing results across multiple studies conducted under different experimental conditions, even when the same method of analysis was applied.

Table 1. Summary of association constants estimated by various approaches a,b in this and other works for alpha-synuclein binding to curved surfaces.

Approximate Diameter (nm)	Ligand / Molar Ratio Phospholipid Components	Cholesterol (mol/mol%)	Method	K _a (Protein into Particles)	K _a (Lipids into Protein)	Source
20 (particle)	Citrate	-	DLS	$2.0 \pm 0.4 \times 10^7 \mathrm{M}^{-1}$	-	Ref ⁴³
90 (particle)	Citrate	-	DLS	$1.8 \pm 0.2 \times 10^8 \mathrm{M}^{-1}$	-	Ref ⁴³
10-100 (particle)	Sodium dodecyl sulfate	-	DLS	$(2.1-5.9) \times 10^7 \mathrm{M}^{-1}$	-	Ref ²⁶
77 (vesicle)	POPC(1):POPS(1)	-	FCS	-	$1.3 \pm 0.2 \times 10^4 \mathrm{M}^{-1}$	Ref ²¹
116 (vesicle)	POPC(1):POPS(1)	-	FCS	-	$5.9 \pm 0.2 \times 10^3 \mathrm{M}^{-1}$	Ref ²¹
44 (vesicle)	DOPC(2):DOPE(5):DOPS(3)	-	CD	-	$2.7 \pm 0.2 \times 10^3 \mathrm{M}^{-1}$	Ref ³¹
44 (vesicle)	DOPC(2):DOPE(5):DOPS(3)	47	CD	-	$1.0 \pm 0.1 \times 10^3 \mathrm{M}^{-1}$	Ref ³¹
20-25 (vesicle)	DOPC(2):DOPE(5):DOPS(3)	-	CD	-	$2.0 \pm 0.2 \times 10^3 \mathrm{M}^{-1}$	Ref ³²
20-25 (vesicle)	DOPC(2):DOPE(5):DOPS(3)	5	CD	-	$2.5 \pm 1.0 \times 10^3 \mathrm{M}^{-1}$	Ref ³²
20-25 (vesicle)	DOPC(2):DOPE(5):DOPS(3)	10	CD	-	$6.0 \pm 1.0 \times 10^3 \mathrm{M}^{-1}$	Ref ³²
20-25 (vesicle)	DOPC(2):DOPE(5):DOPS(3)	20	CD	-	$3.3 \pm 0.4 \times 10^3 \mathrm{M}^{-1}$	Ref ³²
20-25 (vesicle)	DOPC(2):DOPE(5):DOPS(3)	40	CD	-	$3.2 \pm 0.4 \times 10^3 \mathrm{M}^{-1}$	Ref ³²
40-60 (vesicle)	DOPC(2):DOPE(5):DOPS(3)	-	FCS	-	$1.5 \pm 0.1 \times 10^6 \mathrm{M}^{-1}$	Ref ³²
40-60 (vesicle)	DOPC(2):DOPE(5):DOPS(3)	5	FCS	-	$3.0 \pm 0.5 \times 10^6 \mathrm{M}^{-1}$	Ref ³²
40-60 (vesicle)	DOPC(2):DOPE(5):DOPS(3)	10	FCS	-	$7.2 \pm 0.2 \times 10^6 \mathrm{M}^{-1}$	Ref ³²
40-60 (vesicle)	DOPC(2):DOPE(5):DOPS(3)	20	FCS	-	$2.4 \pm 0.1 \times 10^6 \mathrm{M}^{-1}$	Ref ³²
40-60 (vesicle)	DOPC(2):DOPE(5):DOPS(3)	40	FCS	-	$2.4 \pm 0.1 \times 10^6 \mathrm{M}^{-1}$	Ref ³²
70 (particle)	DOPC(3):DOPE(3):DOPS(1):SM(1)	-	DLS	$5.9 \pm 1.6 \times 10^8 \text{ M}^{-1}$	-	This Work
70 (particle)	DOPC(3):DOPE(3):DOPS(1):SM(1)	20	DLS	$1.7 \pm 0.7 \times 10^9 \mathrm{M}^{-1}$	-	This Work
130 (particle)	DOPC(3):DOPE(3):DOPS(1):SM(1)	-	DLS	$1.8 \pm 0.8 \times 10^{9} \mathrm{M}^{-1}$	-	This Work
130 (particle)	DOPC(3):DOPE(3):DOPS(1):SM(1)	20	DLS	$1.1 \pm 0.7 \times 10^9 \mathrm{M}^{-1}$	-	This Work
70 (vesicle)	DOPC(3):DOPE(3):DOPS(1):SM(1)	-	CD	-	$1.6 \pm 0.7 \times 10^2 \mathrm{M}^{-1}$	This Work
75 (vesicle)	DOPC(3):DOPE(3):DOPS(1):SM(1)	20	CD	-	$4.8 \pm 0.7 \times 10^2 \text{ M}^{-1}$	This Work
115 (vesicle)	DOPC(3):DOPE(3):DOPS(1):SM(1)	-	CD	-	$4.8 \pm 0.8 \times 10^2 \mathrm{M}^{-1}$	This Work
120 (vesicle)	DOPC(3):DOPE(3):DOPS(1):SM(1)	20	CD	-	$4.5 \pm 1.3 \times 10^2 \mathrm{M}^{-1}$	This Work

^aExperiments were carried out either by titrating protein into particles, or by titrating lipids in protein. ^bMethods include titrations by dynamic light scattering (DLS), fluorescence correlation spectroscopy (FCS), and circular dichroism spectroscopy (CD). ^cGold nanoparticles and lipid vesicles of different sizes with membrane mimetic and non-membrane mimetic surface chemistries.

Another barrier to quantitative comparison of binding affinities is the use of different analysis methods in which the fundamental characteristic being measured (e.g., particle size, protein secondary structure, fluorescence autocorrelation) varies as well as the type of concentration used (e.g., total particle, total lipid, accessible lipid) in calculations. Ideally, experimental factors could be standardized between studies or experiments to achieve quantitative comparison, however identifying a single compatible analysis method for mimics with very different characteristics is challenging. For example, dynamic light scattering titrations are appropriate for rigid particles where size increase can be attributed to protein adsorption, but it does not work well for malleable particles that can undergo deformation upon particle binding leading to unpredictable variations in hydrodynamic size (Figure S12). Conversely, circular dichroism titrations and fluorescence correlation spectroscopy are often used successfully with malleable particles (i.e., vesicles), but optical interference of gold nanoparticles precludes them from these approaches (Figure S13). Here we chose to use dynamic light scattering for our rigid lipid-coated gold nanoparticles and circular dichroism (described below) for our malleable phospholipid vesicles. Isothermal titration calorimetry has been used less frequently and with some difficulty to monitor molecule/particle binding, 48,49 but it has been successfully applied to protein/vesicle binding on several occasions^{22,50} and could represent an opportunity to achieve quantitative comparison of binding affinity measurements across diverse membrane model systems in the future using a single unifying analysis approach.

Alpha-Synuclein/Malleable Mimic Binding Affinity by Circular Dichroism Titrations. Because alpha-synuclein is an intrinsically disordered protein in solution that adopts alpha-helical character upon binding to membrane-like surfaces, binding can be monitored *via* circular dichroism spectroscopy by observing changes in ellipticity at 222 nm, one of the wavelengths

indicative of alpha-helical secondary structure. For these experiments, the concentration of alpha-synuclein was kept constant as the amount of phospholipid vesicles added to the protein was increased. Circular dichroism spectra were also taken for each vesicle concentration in the absence of alpha-synuclein. Similarly to previous reports, ^{50,51} the vesicle background was then subtracted from each sample and the change in CD signal at 222 nm was plotted against vesicle concentration (Figure 5). Here, due to the large size of the vesicles in use, the change in ellipticity at 222 nm was calculated from the first titration point (0.01mg/mL lipid) rather than from a free protein measurement (0 mg/mL lipid) to account for vesicle interference that could not be eliminated by background subtraction alone.

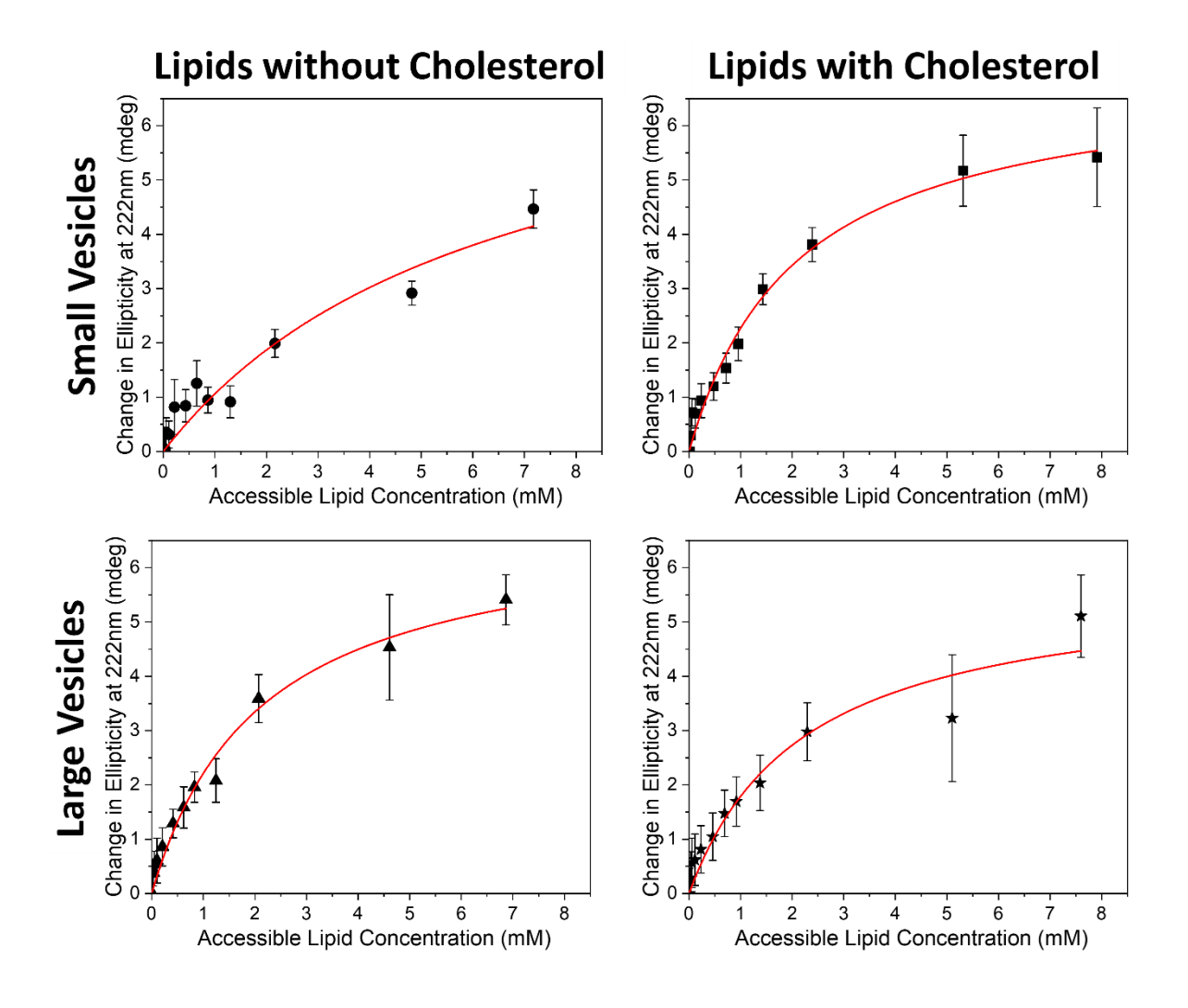


Figure 5. Circular dichroism titrations of alpha-synuclein with phospholipid vesicles. The change in ellipticity at 222 nm is plotted as a function of accessible lipid concentration. The data shown here is an average of three replicate titrations for each condition. Error bars represent the standard deviation of the averaged replicates. Fitting of the data with a Langmuir Adsorption Isotherm is shown in red.

Apparent association constants (K_a) for each phospholipid vesicle/alpha-synuclein pairing were estimated by fitting their respective binding curves using a Langmuir Adsorption Isotherm (**Equation 2**) similarly to the analysis described above. In this case, ΔCD is the change in ellipticity at 222 nm for a given titration point, ΔCD_{max} is the maximum change in ellipticity at 222 nm, and [lipid] is the concentration of accessible lipids for a given titration point.

$$\frac{\Delta CD}{\Delta CD_{max}} = \frac{K_a[lipid]}{1 + K_a[lipid]}$$
 (Equation 2)

The plateau values for all titrations, falling at a change in ellipticity of approximately 5 millidegrees, is in good agreement with values obtained for a series of control samples (**Figure S14**). Estimated association constants (**Table 1**) for large phospholipid vesicles with and without cholesterol as well as small phospholipid vesicles with cholesterol all fell in the range of (4.5-4.8) × 10² M⁻¹. However, similarly to the trend observed for lipid-coated gold nanoparticles, small phospholipid vesicles without cholesterol yielded a slightly lower association constant of 1.6 × 10² M⁻¹. These results indicate that both malleable and rigid mimics experience decreased binding affinity under the combined absence of cholesterol and decrease in particle size, whereas no significant change in binding affinity is observed for changes in mimic size or lipid composition alone. Previous studies investigating the role of cholesterol in alpha-synuclein binding affinity to phospholipid vesicles have yielded contradicting results (**Table 1**). While Man *et al.* observed a linear decrease in binding affinity with increasing cholesterol content up to nearly 50 mol%, ³¹ Mahapatra *et al.* reported an increase in binding affinity upon the addition of 5-40 mol% cholesterol with the strongest binding occurring at a composition of 10 mol% cholesterol.

Comparing just our small phospholipid vesicle conditions, we observe a trend similar to that reported by Mahapatra *et al.* in which addition of cholesterol results in an increase in binding affinity. Interestingly, we do not observe a trend in either direction for the large phospholipid vesicle samples, suggesting that the ability of cholesterol content to influence binding affinity, possibly through modulating lipid packing defects, 44,45 is less significant for larger vesicles with lower surface curvature.

Protein Binding Orientation by Limited Proteolysis Mass Spectrometry Analysis. The binding orientation of alpha-synuclein to the surface of our rigid and malleable synaptic vesicle mimics was probed using a limited proteolysis approach (Scheme S2, Figure S15). Each synaptic vesicle mimic was incubated with sufficient alpha-synuclein to achieve approximately monolayer surface coverage as estimated by DLS and CD titration experiments. Partial enzymatic digestion was then achieved by employing Glu-C at a low enzyme to protein ratio (1:200 by mass) and low digestion temperature (25°C), similarly to previous studies. Protein fragments released from the surface of the mimics upon digestion were then isolated and analyzed by mass spectrometry with label free quantification (LFQ) performed by MaxQuant. This analysis method allows for the determination of relative amounts of each protein fragment across all samples. Under these conditions, we expected fragments from accessible, solvent-exposed regions of the protein to be detected more frequently, while fragments from less accessible, protected regions of the protein should be detected less frequently.

Fragmentation patterns for free alpha-synuclein and alpha-synuclein digested from the surface of either malleable or rigid synaptic vesicle mimics all showed full sequence coverage (Figure 6, Figure S16). Furthermore, the presence of fragments across all sample types in which

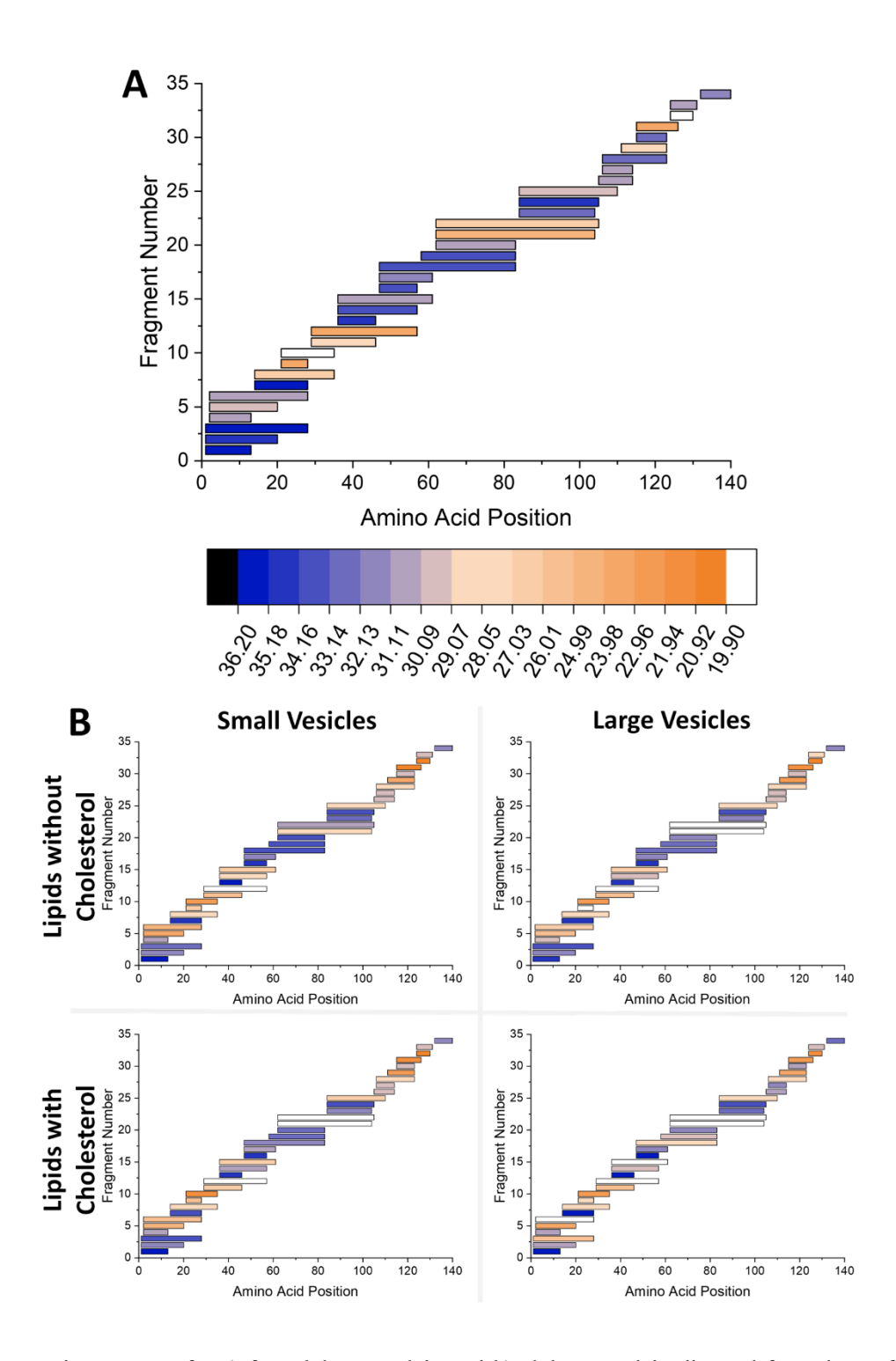


Figure 6. Fragmentation patterns for a) free alpha-synuclein and b) alpha-synuclein digested from the surface of malleable, phospholipid vesicles by Glu-C. Each bar represents a protein fragment detected by mass spectrometry and the color scale indicates the log₂ value of the average LFQ intensity obtained for a given fragment across three replicate samples [high LFQ (blue), low LFQ (orange)]. Bars that are white indicate fragments that were not detected for a certain condition but were detected in other conditions.

1-2 digestion sites were missed indicates that we are in fact operating under partial rather than complete digestion conditions. The most commonly detected fragments, as indicated by high LFQ intensity, for free alpha-synuclein were primarily located at the N-terminal of the protein sequence. Fragments originating from the region between residues 36-105 were the next most common, while fragments in the range of residues 29-35 were the least common. Similar overarching trends were observed in the fragmentation patterns of alpha-synuclein digested from the surface of rigid synaptic vesicle mimics (Figure S16), however fragments in the N-terminal and C-terminal regions of these samples typically showed lower LFQ intensities than the free protein which could indicate that they are released less frequently from the rigid mimic's surface and are therefore more protected from digestion when bound. Interestingly, alpha-synuclein digested from the surface of malleable synaptic vesicle mimics demonstrated more significant differences in fragmentation patterns when compared to free alpha-synuclein. Namely, several longer fragments containing missed cleavage sites were not detected in malleable mimic conditions except in the case of the small vesicles not containing cholesterol (**Figure 6**). Most notably, fragments 62-104 and 62-105, which are missing from most malleable mimic conditions, are detected at a higher rate in the small vesicle condition not containing cholesterol when compared to free alpha-synuclein. Significantly, the small vesicle condition not containing cholesterol also demonstrated a decreased binding affinity compared to the other malleable conditions, suggesting a connection between weaker alpha-synuclein binding and increased detection of released alpha-synuclein fragments from this region of the protein.

To explore these observed trends in more detail, we also considered the digestion patterns of alpha-synuclein from the perspective of the specific cut sites (**Figure 7**). In order to achieve this, the LFQ intensities for each fragment were first averaged across replicates of a given

condition, only considering fragments that had LFQ intensities recorded for 2 or more replicates. The averaged LFQ intensities for all fragments associated with a given digestion site were then summed. Finally, the fold change between free and bound was calculated by taking log₂ of the ratio of the summed LFQ intensities for bound protein/free protein. Values below zero indicate regions of the bound protein that are less accessible to digestion compared to free protein, while values above zero indicate regions of the bound protein that are more accessible to digestion compared to free protein. Across all mimic types, the N-terminal region of the protein was found to be more protected from digestion in comparison to free protein, demonstrating approximately 2-fold decrease in associated LFQ intensity at residue 20 for rigid mimic samples and up to 3.5fold decrease for malleable mimic samples at the same digestion site. This observation agrees with the results of our previous investigation into alpha-synuclein binding to rigid, SDS-based synaptic vesicle mimics²⁶ and aligns with the expectation that alpha-synuclein binds to membrane surfaces via an amphipathic alpha-helical structure that forms in the N-terminal region of the protein. 9,12,52 Interestingly, in the C-terminal region of alpha-synuclein, residues 115-126 were also found to be protected from digestion in comparison to free protein, differing from our previous study²⁶ and other reports of a free floating C-terminal region upon membrane binding.⁵² Furthermore, the final fragment, comprising residues 132-140, showed an approximate 1-fold increase in LFQ intensity for large and small rigid mimics without cholesterol, which was not observed in other mimic conditions.

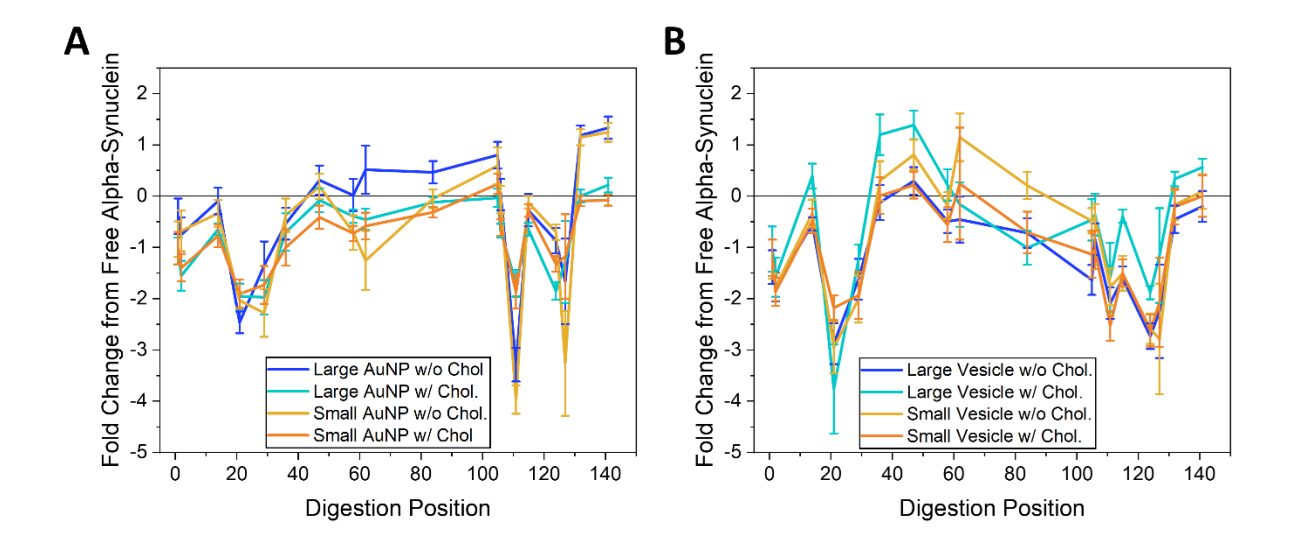


Figure 7. Difference digestion patterns between free alpha-synuclein and alpha-synuclein bound to a) lipid-coated gold nanoparticles or b) extruded lipid vesicles. The fold change was calculated by taking log₂ of the ratio of the summed LFQ intensities for fragments associated with a given digestion site in bound protein/free protein. Values below zero indicate regions of the bound protein that are less accessible to digestion compared to free protein, while values above zero indicate regions of the bound protein that are more accessible to digestion compared to free protein. Error bars represent the standard deviation based on data collected from triplicate samples.

For rigid mimics (Figure 7A), digestion in the central NAC region of the protein is fairly similar to that observed for the free protein, with only a mild exposure observed for large gold nanoparticles without cholesterol and a mild protection observed around residue 61 for the other rigid mimic conditions. In our previously studied surfactant-based mimic system, wildtype alphasynuclein bound to larger (65-100 nm) SDS-coated gold nanoparticles similar in size to our current system also behaved very similarly to free protein, while more significant exposure in the NAC region for was only observed for smaller (10-50 nm) mimics. ²⁶ This suggests that low surface curvature could help prevent exposure of the NAC region upon membrane binding. For malleable mimics (Figure 7B), mild protection was observed at the end of the NAC region from residues 83-104 for all conditions except for small vesicles without cholesterol which shows mild exposure at the beginning of the NAC region from residues 61-83. Furthermore, residues 36-47 were exposed upon binding to large vesicles with cholesterol and, to a lesser extent, small vesicles

without cholesterol. Interestingly, this region encompasses a short motif (*i.e.*, residues 36-42) that was found to play an important role in alpha-synuclein aggregation and function.⁵³

Finally, we investigated the hypothesis that the observed dipping behavior in our DLS binding curves could be due to a change in alpha-synuclein display on the surface of the particles at higher protein concentrations. Small lipid-coated gold nanoparticles without cholesterol, chosen as the exemplary mimic condition for this experiment, were incubated with alpha-synuclein at protein-to-particle ratios corresponding to the peak and dip regions of the titration curve for analysis by limited proteolysis mass spectrometry (**Figure 8**). Samples prepared at both incubation ratios were washed of any free, unbound protein prior to analysis. We found that the central NAC region and portions of the C-terminus were more exposed in the dip condition compared to the

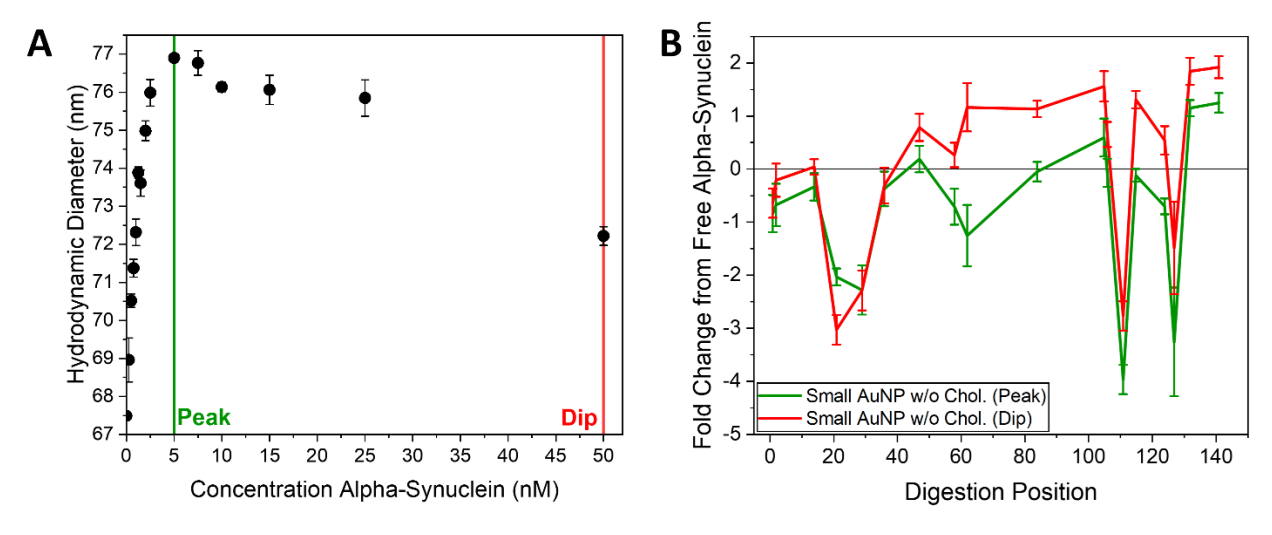


Figure 8. Comparison of alpha-synuclein binding behavior in the peak (green) and dip (red) regions of a) a representative DLS titration curve for small lipid-coated gold nanoparticles without cholesterol. Small lipid-coated gold nanoparticles without cholesterol were incubated with alpha-synuclein at protein-to-particle ratios corresponding to the peak and dip regions of the titration curve for analysis by limited proteolysis mass spectrometry to obtain b) the difference in digestion patterns between free alpha-synuclein and alpha-synuclein bound to small lipid-coated gold nanoparticles without cholesterol at different incubation ratios. The fold change was calculated by taking log₂ of the ratio of the summed LFQ intensities for fragments associated with a given digestion site in bound protein/free protein. Values below zero indicate regions of the bound protein that are less accessible to digestion compared to free protein, while values above zero indicate regions of the bound protein that are more accessible to digestion compared to free protein. Error bars represent the standard deviation based on data collected from triplicate samples.

peak condition. These results indicate that protein-to-particle incubation ratio plays a role in determining protein orientation upon binding to these rigid mimics which could contribute to the non-traditional shape of their binding curves.

CONCLUSIONS

In this study we developed a library of synaptic vesicle mimics comprising a range of both malleable phospholipid vesicles and rigid lipid-coated gold nanoparticles of two distinct sizes. While quantification of lipid composition in the final synthesized mimics posed several challenges, results suggested that the molar ratios of components present across all mimic conditions were comparable. Upon interaction of alpha-synuclein with all mimic types, limited proteolysis experiments showed that the N-terminal region of the protein became protected against digestion consistent with the reported membrane binding region. Much of the C-terminal region of alphasynuclein became protected against digestion as well, although this observation is in contrast with studies which typically depict alpha-synuclein's C-terminal end as a free-floating tail, which has little to no interaction with membrane surfaces upon binding. Interestingly, higher binding affinities were observed for alpha-synuclein binding to rigid synaptic vesicle mimics compared to malleable synaptic vesicle mimics. Furthermore, the small lipid-coated gold nanoparticles and small lipid vesicles without cholesterol stood out amongst all the mimic conditions as they demonstrated lower binding affinities toward alpha-synuclein than their respective rigid and malleable counterparts. The small lipid vesicles without cholesterol also had a different digestion pattern than the other malleable mimics, displaying exposure rather than protection in the NAC region. Finally, differences in alpha-synuclein orientation on the surface of rigid synaptic vesicle mimics at different protein-to-particle incubation ratios are believed to contribute to the nontraditional peak and dip shape of the observed binding curves. Increased exposure of the NAC region at higher protein concentrations could possibly act as a seed for pathogenic alpha-synuclein aggregation.

MATERIALS AND METHODS

Tetrachloroauric(III) acid trihydrate (HAuCl₄·3H₂O), hydroquinone, 1-octadecanethiol, sodium dodecyl sulfate, chloroform, HEPES, and ammonium bicarbonate were purchased from Sigma-Aldrich; cholesterol (ovine wool, powder, 98%), 1,2-dioleoyl-sn-glycero-3phosphocholine (DOPC, 25mg/mL in chloroform), 1,2-dioleoyl-sn-glycero-3phosphoethanolamine (DOPE, 25mg/mL in chloroform), 1,2-dioleoyl-sn-glycero-3-phospho-Lserine (DOPS, sodium salt, 25mg/mL in chloroform) and sphingomyelin (porcine brain, 25mg/mL in chloroform) were purchased from Avanti Polar Lipids; potassium cyanide was purchased from Fluka BioChemika; osmium tetroxide (4% solution) was purchased from Electron Microscopy Sciences; trisodium citrate dihydrate (Na₃C₆H₅O₇·2H₂O) was purchased from Flinn Scientific; sodium hydroxide was purchased from Fisher Scientific; Glu-C endoproteinase was purchased from Thermo Scientific. All materials were used without further purification. Extinction spectra were collected on a Cary 5000 UV-vis-NIR spectrophotometer, transmission electron microscopy images were collected on a JEOL 2100 CRYO TEM, dynamic light scattering measurements were taken on a Malvern Panalytical Zetasizer Nano-ZS, circular dichroism spectra were collected on an Olis DSM17. Exo-spinTM mini-HD columns were obtained from Cell Guidance Systems. Water used in all preparations was obtained from a Barnstead NANOpure II water purification system.

Synthesis of Lipid Vesicles. Lipid vesicles were synthesized by extrusion using an Avanti Mini Extruder at room temperature. First, the desired molar ratio of lipids in chloroform were combined, mixed well, and dried down under a stream of nitrogen. A molar ratio of either 3:3:1:1:2 DOPC:DOPE:DOPS:sphingomyelin:cholesterol or 3:3:1:1 DOPC:DOPE:DOPS:sphingomyelin was used for all experiments. The resulting lipid film was then placed under vacuum overnight to remove any remaining solvent traces. The lipids were then rehydrated to a desired concentration in the range of 1 mg/mL to 10 mg/mL with HEPES buffer (10 mM, pH 7) or ammonium bicarbonate (10 mM, pH 8) and allowed to agitate on a shaker for ~1 hr to form a milky white solution containing large multilamellar vesicles. This solution was briefly vortexed before proceeding. The resulting solution was loaded into a syringe and passed through a single polycarbonate membrane of defined pore size 31 times, ending with the lipid solution in the alternate syringe. To obtain large vesicles the solution was passed through a membrane with 100 nm pores. To obtain small vesicles the solution was passed first through a membrane with 100 nm pores, then 50 nm pores, and finally 30 nm pores in a step-down approach. The sizes of the resulting lipid vesicles were characterized by dynamic light scattering. As synthesized lipid vesicles were stored in the refrigerator at 20°C for up to 7 days.

Synthesis of Citrate-Capped Gold Nanoparticles. Small and large gold nanoparticles were synthesized according to a previously reported method.⁵⁴ First, a seed solution was made by bringing 50 mL water and 500 μL 1% w/v HAuCl₄ to a boil under stirring, followed by the addition of 1.5 mL 1% w/v sodium citrate. The resulting solution was allowed to boil for 10 minutes, during which time it underwent a color change from clear to pink to red and was then cooled to room temperature. Small ~50 nm (and large ~120 nm) gold nanoparticles were grown at room temperature by combining 239.5 mL (243.8mL) water, 2.5 mL 1% w/v HAuCl₄, 5 mL (0.4 mL)

seeds, $550 \mu L$ 1% w/v sodium citrate, and 2.5 mL 0.03 M hydroquinone under stirring for 1 hr. Gold nanoparticles were collected by centrifugation at 600g for 30 min (200g for 30 min). The resulting nanoparticles were characterized by UV-vis, dynamic light scattering, and transmission electron microscopy.

Lipid-Coating of Gold Nanoparticles. After synthesis, the citrate-capped gold nanoparticles were coated with a hybrid lipid bilayer based on a previously established protocol³⁸ which utilizes an inner alkane thiol layer as an anchor to facilitate the association of an outer lipid layer to the particle surface. To achieve small lipid-coated gold nanoparticles, 0.022 nmol small citrate-capped gold nanoparticles were combined first with 22 mg lipids (rehydrated as described above), followed by the addition of 4.4 mg octadecane thiol (from 10 mg/mL ethanolic stock solution) in a total incubation volume of approximately 4.5 mL HEPES buffer (10 mM, pH 7). For large lipidcoated gold nanoparticles, 0.0034 nmol large citrate-capped gold nanoparticles were combined first with 17 mg lipids (rehydrated as described above), followed by the addition of 6.8 mg octadecane thiol (from 10 mg/mL ethanolic stock solution) in a total incubation volume of approximately 4.7 mL HEPES buffer (10 mM, pH 7). These mixtures were then sonicated for 10 minutes and allowed to incubate on a shaker at room temperature overnight. The following day, samples were centrifuged two times to remove any excess lipids remaining in solution. Samples with small particles were centrifuged at 600g for 30 minutes, while samples with large particles were centrifuged at 200g for 30 minutes.

Cyanide Etching of (Lipid-Coated) Gold Nanoparticles. A solution of 100 mM potassium cyanide was made using 0.1 mM sodium hydroxide. Citrate-capped gold nanoparticles or lipid-coated gold nanoparticles were prepared at an appropriate dilution for measurement by UV-vis using 0.1 mM sodium hydroxide in a 1 cm quartz cuvette. An aliquot of the as prepared potassium

cyanide solution was then added to the particles in the cuvette, the cuvette was capped, and the extinction of the sample was monitored by UV-vis spectroscopy for changes over time. Potassium cyanide was added to gold nanoparticle samples in an amount sufficient to achieve at least a 10x stoichiometric excess of cyanide ions to gold atoms. Safety Note: Solutions of potassium cyanide should be maintained under basic conditions and never mixed with acidic solutions in order to prevent the formation of highly toxic hydrogen cyanide.

Osmium Tetroxide Staining of Lipid-Coated Gold Nanoparticles. The staining procedure was adapted from a previously reported approach.³⁸ Briefly, 10 µL of lipid-coated gold nanoparticles at half their synthesized concentration were dropcast onto a TEM grid and allowed to dry overnight. The grid was then floated sample side down on top of a 0.4% osmium tetroxide solution for 1 hour. Finally, the grid was rinsed sample side down in water 3 times for 10 minutes. The grid was allowed to dry sample side up on a piece of filter paper and then taken immediately for TEM imaging.

Analysis of Lipid Composition. The composition of lipids present in final synaptic vesicle mimics was assessed according to Scheme S1. DOPC, DOPE, and DOPS were quantified by liquid chromatography-mass spectrometry (LC-MS). Cholesterol was quantified using a fluorometric Cholesterol Quantification Assay Kit (CS0005) obtained from Sigma Aldrich. Total phosphorus concentration was determined by colorimetric assay according to a procedure published by Avanti Polar Lipids⁵⁵ or by inductively coupled plasma-mass spectrometry (ICP-MS).

Extraction of lipids from the surface of coated gold nanoparticles was achieved using a modified approach to the Folch method^{40,41} by first adding 2 mL of sample in 10 mM HEPES buffer to 8 mL of a 2:1 chloroform:methanol mixture. Samples were then vortexed in 1 minute intervals for a total of 3 minutes. The phases were allowed to separate for ~30 min, then the organic

layer containing extracted lipids was collected. Fresh organic phase was added and samples were extracted two additional times. Collected organic layers for each sample were dried down by rotovap and placed under vacuum for 1 hr to remove trace solvent. Finally, extracted lipids were rehydrated in 10 mM HEPES for 1 hr before analysis.

Expression and Purification of Alpha-Synuclein. Wildtype alpha-synuclein protein was expressed and purified as previously described.⁵⁶ Final protein stock solutions used for experimentation had a concentration of 11.01 mg/mL (761 μM) wildtype alpha-synuclein in 1 mM EDTA, 10 mM Tris-HCl, and 150 mM NaCl (pH 8).

Dynamic Light Scattering Titrations. First, a working solution of 0.5 μM alpha-synuclein was made by diluting 1 μL of the 761 μM stock solution to a final volume of 1.5 mL using 10 mM HEPES buffer (pH 7). Titration curves were collected for protein concentrations ranging from 0-50 nM alpha-synuclein added to constant concentrations of either 0.025 nM small lipid-coated gold nanoparticles or 0.0075 nM large lipid-coated nanoparticles in a total volume of 1 mL 10 mM HEPES buffer (pH 7). Each titration point for a given curve was prepared simultaneously in separate microfuge tubes, and the samples were allowed to incubate on a shaker for at least 30 minutes before collecting DLS measurements. The order of titration point measurement was randomized within each replicate curve to account for any potential impact of varied incubation time. Three measurements of ~15 scans each were taken and averaged for each titration point. Each titration curve was conducted in triplicate. All DLS measurements of hydrodynamic size were obtained by cumulants fitting.

Circular Dichroism Titrations. Titration curves were collected for vesicle concentrations providing 0-8 mM accessible lipids added to a constant concentration of 2 μM alpha-synuclein in a final volume of 0.3 mL 10 mM HEPES buffer (pH 7). Accessible lipids are considered those in

the outer leaflet and their concentration was determined geometrically based on vesicle hydrodynamic size and previously published calculations. ²¹ Each titration point for a given curve was prepared simultaneously in separate microfuge tubes, and the samples were allowed to incubate on a shaker for at least 30 min before collecting circular dichroism measurements. The order of titration point measurement was randomized within each replicate curve to account for any potential impact of varied incubation time. Five scans were taken and averaged for each titration point with an integration time of 1 second and increments of 0.1 nm over the range of 220-224 nm, bandwidth 8. The resulting spectra were smoothed using a Savitsky-Golay filter and the change in ellipticity at 222 nm (representative of alpha-helical secondary structure) was monitored. Vesicle control scans were taken at each vesicle concentration, and any signal originating from the vesicles on their own was background subtracted from the respective samples. Each titration curve was conducted in triplicate. Full spectra of select samples were also taken over the range of 200-250 nm with 0.2 nm increments.

Enzymatic Digestion and Separation of Alpha-Synuclein from the Surface of Lipid-Coated Gold Nanoparticles. In a typical digest (Scheme S2A), 20 μg alpha-synuclein was incubated with 0.007 nmol small lipid-coated particles or 0.001 nmol large lipid-coated particles in 600 μL total volume (10 mM ammonium bicarbonate, pH 8) at 4 °C overnight. Small and large lipid-coated particle concentrations were selected to achieve approximately monolayer surface coverage upon protein incubation, as estimated from DLS titration data. The surface area of the gold nanoparticle cores was kept constant between samples. After protein incubation, samples were centrifuged twice to remove any excess unbound protein. Samples with small particles were centrifuged at 600g for 30 min, while samples with large particles were centrifuged at 200g for 30 min. After the first centrifugation step, 550 μL of supernatant was removed and replaced with an equal volume

of 10 mM ammonium bicarbonate (pH 8). After the second centrifuge step, 550 μL supernatant was removed and replaced with 540 μL ammonium bicarbonate plus 10 μL Glu-C endoproteinase (10 μg/mL). Enzymatic digestion was then allowed to take place for 6 hr in a 25 °C water bath. Glu-C digestion sites are identified in **Figure S15.** Finally, the digested samples were centrifuged to pellet all gold nanoparticles, and the top 550 μL of the supernatant containing protein fragments released due to digestion were collected. The collected samples were immediately placed in the freezer at -20 °C for overnight storage before submission for mass spectrometry analysis the following day. Free protein controls were conducted by adding 20 μg alpha-synuclein and 100 ng Glu-C Endoproteinase directly into a total volume of 600 μL ammonium bicarbonate (10 mM, pH 8) and allowing digestion to take place for 6 hr in a 25 °C water bath without the need for centrifugation steps.

Enzymatic Digestion and Separation of Alpha-Synuclein from the Surface of Lipid Vesicles. In a typical digest (Scheme S2B), 20 μg alpha-synuclein was incubated with 1 mg small lipid vesicles or 1 mg large lipid vesicles in 150 μL total volume (10 mM ammonium bicarbonate, pH 8) at 4 °C overnight. After protein incubation, samples were passed through an ExoSpinTM mini-HD size exclusion chromatography column in order to remove any excess unbound protein. First, columns were brought to room temperature, storage buffer was removed, and the columns were flushed three times with 2.5 mL ammonium bicarbonate (10 mM, pH 8). Next, the 150 μL sample volume was applied to the top of the column. Once the sample had entered the column, 50 μL of ammonium bicarbonate was added and the first fraction totaling 200 μL was collected by gravity. Next, 200 μL ammonium bicarbonate was applied to the top of the column and collected by gravity as the second fraction. This process was repeated a further 22 times until a total of 24 fractions of approximately 200 μL had been collected. A 2 μL aliquot of each fraction was analyzed by

Nanodrop and fractions containing vesicles (typically fractions 5-8 as determined by signal arising from vesicle scattering) were saved and combined. These combined fractions were concentrated under vacuum to a volume of approximately 140 μL before proceeding. Next, 10 μL Glu-C endoproteinase (10 µg/mL) was added to the samples and enzymatic digestion was then allowed to take place for 6 hr in a 25 °C water bath. Glu-C digestion sites are identified in Figure S15. Finally, digested samples were passed through an ExoSpinTM mini-HD size exclusion chromatography column according to the procedure described above in order to separate protein fragments released from the vesicle surface due to digestion from protein fragments which remained bound. In this case, fractions containing free protein but not containing lipid vesicles (typically fractions 16-20) were saved and combined. The combined fractions were immediately placed in the freezer at -20 °C for overnight storage before submission for mass spectrometry analysis the following day. Free protein controls were conducted by adding 20 µg alpha-synuclein and 100 ng Glu-C Endoproteinase directly into a total volume of 600 µL ammonium bicarbonate (10 mM, pH 8) and allowing digestion to take place for 6 hr in a 25 °C water bath without the need for centrifugation steps.

Mass Spectrometry and Proteomics. Peptide samples were desalted using StageTips, and the amount in each sample was determined with a Pierce quantitative colorimetric peptide (modified BCA) assay. The dried peptides were suspended in a solution of 0.1% formic acid (FA) in 5% acetonitrile (ACN), and 30 ng from each sample was injected into an UltiMate 3000 RSLCnano system. The peptides were separated using a 25 cm Acclaim PepMap 100 C18 column (Thermo Scientific) and mobile phases of 0.1% FA (A) and 0.1% FA in 80% ACN (B) at a flow rate of 300 nL/min. The gradient started at 5% B, increased to 35% B over 40 minutes, and then increased to

50% B over 5 more minutes; this was followed by column washing and equilibration. The column was maintained at 50 °C over the course of the run.

The peptides were analyzed with a Q Exactive HF-X mass spectrometer (Thermo Scientific) in positive mode. MS1 scans from 350 to 1500 m/z were acquired at 120k resolution (3e6 AGC; 60 ms max IT), followed by HCD fragmentation (30 NCE) of the 15 most abundant ions. MS2 scans were acquired at 30k resolution with an isolation window of 1.0 m/z and a dynamic exclusion time of 20 s (5e4 AGC; 35 ms max IT).

The raw LC-MS data was searched against the Uniprot Homo sapiens reference proteome (78,806 entries) with MaxQuant v2.0.1.0. GluC was specified as the enzyme with a maximum of 2 missed cleavages; minimum peptide length was set to 6. Variable modifications of methionine oxidation and N-terminal acetylation were also added to the search. The precursor mass tolerance was 20 ppm for the first search and 10 ppm for the main search, while the fragment mass tolerance was set to 20 ppm. The match between runs function was enabled with a match time window of 1 min, and the false discovery rate was set to 1% at the PSM and protein levels. Label-free quantitation was also performed with MaxQuant using a minimum ratio count of two.

ASSOCIATED CONTENT

Supporting Information. Transmission electron microscopy images of citrate-capped gold nanoparticles, size distributions of citrate-capped gold nanoparticles, summary of hydrodynamic diameters for all particles used in experiments, summary of zeta potentials for all particles used in experiments, osmium tetroxide staining of lipid-coated gold nanospheres with cholesterol, osmium tetroxide staining of lipid-coated gold nanospheres without cholesterol, experimental approach to lipid quantification, lipid composition on coated gold nanoparticles after extraction, ³¹P-detected

SSNMR experiments, dynamic light scattering titration with cyanide etching, dynamic light scattering titration with and without centrifugation, dynamic light scattering titrations with artificial plateau, dynamic light scattering titration of small lipid vesicles without cholesterol, circular dichroism spectra of alpha-synuclein under different binding conditions, circular dichroism of alpha-synuclein with sodium dodecyl sulfate, limited proteolysis mass spectrometry workflow, Glu-C digestion locations, fragmentation patterns for alpha-synuclein digested from lipid-coated gold nanoparticles. (PDF)

AUTHOR INFORMATION

Corresponding Author

*Catherine J. Murphy – Department of Chemistry, University of Illinois at Urbana-Champaign, Urbana, Illinois 61801, United States; Email: murphycj@illinois.edu

Author Contributions

This manuscript was written through contributions of all authors.

Notes

The authors declare no competing financial interests.

ACKNOWLEDGMENTS

Contributions from S.M.M. were supported by the National Science Foundation under Grant No. CHE-2107793, by the NIH Chemistry–Biology Interface Training Grant No. T32-GM136629, and by the National Science Foundation Graduate Research Fellowship Program. This work is further supported by NIH Grant No. P41GM136463 and NIH Grant No. U01NS110436. Transmission electron microscopy characterization of gold nanoparticles was carried out in the Materials

Research Laboratory Central Facilities at the University of Illinois, Urbana-Champaign. Proteomics analysis was conducted with assistance from the Proteomics Core Facility of the Roy J. Carver Biotechnology Center at the University of Illinois, Urbana-Champaign. Lipid quantification by LC-MS was conducted by the Metabolomics Core Facility of the Roy J. Carver Biotechnology Center at the University of Illinois, Urbana-Champaign.

REFERENCES

- Spillantini, M. G.; Schmidt, M. L.; Lee, V. M.-Y.; Trojanowski, J. Q.; Jakes, R.; Goedert,
 M. Alpha -Synuclein in Lewy Bodies. *Nature* 1997, 388, 839–840.
- (2) Goedert, M.; Jakes, R.; Spillantini, M. G. The Synucleinopathies: Twenty Years On. *Journal of Parkinson's Disease.* **2017**, *7*, S51-S69.
- (3) Weinreb, P. H.; Zhen, W.; Poon, A. W.; Conway, K. A.; Lansbury, P. T. NACP, a Protein Implicated in Alzheimer's Disease and Learning, Is Natively Unfolded. *Biochemistry* 1996, 35 (43), 13709–13715.
- (4) Theillet, F. X.; Binolfi, A.; Bekei, B.; Martorana, A.; Rose, H. M.; Stuiver, M.; Verzini, S.; Lorenz, D.; Van Rossum, M.; Goldfarb, D.; *et al.* Structural Disorder of Monomeric alpha-synuclein Persists in Mammalian Cells. *Nature* **2016**, *530* (7588), 45–50.
- (5) Giasson, B. I.; Murray, I. V. J.; Trojanowski, J. Q.; Lee, V. M. Y. A Hydrophobic Stretch of 12 Amino Acid Residues in the Middle of alpha-synuclein Is Essential for Filament Assembly. *J. Biol. Chem.* **2001**, *276* (4), 2380–2386.
- (6) Du, H.-N.; Tang, L.; Luo, X.-Y.; Li, H.-T.; Hu, J.; Zhou, J.-W.; Hu, H.-Y. A Peptide Motif Consisting of Glycine, Alanine, and Valine Is Required for the Fibrillization and

- Cytotoxicity of Human R-Synuclein. *Biochemistry* **2003**, *42*, 8870-8878.
- (7) Tuttle, M. D.; Comellas, G.; Nieuwkoop, A. J.; Covell, D. J.; Berthold, D. A.; Kloepper, K. D.; Courtney, J. M.; Kim, J. K.; Barclay, A. M.; Kendall, A.; et al. Solid-State NMR Structure of a Pathogenic Fibril of Full-Length Human alpha-synuclein. Nat. Struct. Mol. Biol. 2016, 23 (5), 409–415.
- (8) Khammari, A.; Shahriar Arab, S.; Reza Ejtehadi, M. The Hot Sites of alpha-synuclein in Amyloid Fibril Formation. *Scientific Reports* **2020**, *10*, 12175.
- (9) Davidson, W. S.; Jonas, A.; Clayton, D. F.; George, J. M. Stabilization of alpha-synuclein Secondary Structure upon Binding to Synthetic Membranes. *J. Biol. Chem.* 1998, 273 (16), 9443–9449.
- (10) Eliezer, D.; Kutluay, E.; Bussell, R.; Browne, G. Conformational Properties of alphasynuclein in Its Free and Lipid-Associated States. *J. Mol. Biol.* **2001**, *307* (4), 1061–1073.
- (11) Dikiy, I.; Eliezer, D. Folding and Misfolding of Alpha-Synuclein on Membranes. *Biochimica et Biophysica Acta Biomembranes*. **2012**, *1818* (4), 1013-1018.
- (12) Auluck, P. K.; Caraveo, G.; Lindquist, S. alpha-synuclein: Membrane Interactions and Toxicity in Parkinson's Disease. *Annual Reviews* **2010**, *26*, 211–233.
- (13) Man, W. K.; Tahirbegi, B.; Vrettas, M. D.; Preet, S.; Ying, L.; Vendruscolo, M.; De Simone, A.; Fusco, G. The Docking of Synaptic Vesicles on the Presynaptic Membrane Induced by alpha-synuclein Is Modulated by Lipid Composition. *Nat. Commun.* 2021, 12 (1), 927.
- (14) Nemani, V. M.; Lu, W.; Berge, V.; Nakamura, K.; Onoa, B.; Lee, M. K.; Chaudhry, F. A.;

- Nicoll, R. A.; Edwards, R. H. Increased Expression of alpha-synuclein Reduces

 Neurotransmitter Release by Inhibiting Synaptic Vesicle Reclustering after Endocytosis.

 Neuron 2010, 65 (1), 66–79.
- (15) Murphy, D. D.; Rueter, S. M.; Trojanowski, J. Q.; Lee, V. M. Y. Synucleins Are Developmentally Expressed, and alpha-synuclein Regulates the Size of the Presynaptic Vesicular Pool in Primary Hippocampal Neurons. *J. Neurosci.* 2000, 20 (9), 3214–3220.
- (16) Burré, J. The Synaptic Function of alpha-synuclein. *J. Parkinsons. Dis.* **2015**, *5* (4), 699–713.
- (17) Flagmeier, P.; Meisl, G.; Vendruscolo, M.; Knowles, T. P. J.; Dobson, C. M.; Buell, A. K.; Galvagnion, C. Mutations Associated with Familial Parkinson's Disease Alter the Initiation and Amplification Steps of alpha-synuclein Aggregation. *Proc. Natl. Acad. Sci. U. S. A.* 2016, *113* (37), 10328–10333.
- (18) Ruf, V. C.; Nübling, G. S.; Willikens, S.; Shi, S.; Schmidt, F.; Levin, J.; Bötzel, K.; Kamp, F.; Giese, A. Different Effects of alpha-synuclein Mutants on Lipid Binding and Aggregation Detected by Single Molecule Fluorescence Spectroscopy and ThT Fluorescence-Based Measurements. *ACS Chem. Neurosci.* **2019**, *10* (3), 1649–1659.
- (19) Ferreon, A. C. M.; Gambin, Y.; Lemke, E. A.; Deniz, A. A. Interplay of alpha-synuclein Binding and Conformational Switching Probed by Single-Molecule Fluorescence. *Proc. Natl. Acad. Sci. U. S. A.* **2009**, *106* (14), 5645–5650.
- (20) Trexler, A. J.; Rhoades, E. alpha-synuclein Binds Large Unilamellar Vesicles as an Extended Helix. *Biochemistry* **2009**, *48* (11), 2304–2306.

- (21) Middleton, E. R.; Rhoades, E. Effects of Curvature and Composition on alpha-synuclein Binding to Lipid Vesicles. *Biophys. J.* **2010**, *99* (7), 2279–2288.
- (22) Nuscher, B.; Kamp, F.; Mehnert, T.; Odoy, S.; Haass, C.; Kahle, P. J.; Beyer, K. alphasynuclein Has a High Affinity for Packing Defects in a Bilayer Membrane: A Thermodynamics Study. *J. Biol. Chem.* **2004**, *279* (21), 21966–21975.
- (23) Kjaer, L.; Giehm, L.; Heimburg, T.; Otzen, D. The Influence of Vesicle Size and Composition on alpha-synuclein Structure and Stability. *Biophys. J.* **2009**, *96* (7), 2857–2870.
- (24) Jensen, P. H.; Nielsen, M. S.; Jakes, R.; Dotti, C. G.; Goedert, M. Binding of alphasynuclein to Brain Vesicles Is Abolished by Familial Parkinson's Disease Mutation. *J. Biol. Chem.* **1998**, *273* (41), 26292–26294.
- (25) Choi, W.; Zibaee, S.; Jakes, R.; Serpell, L. C.; Davletov, B.; Anthony Crowther, R.; Goedert, M. Mutation E46K Increases Phospholipid Binding and Assembly into Filaments of Human alpha-synuclein. *FEBS Lett.* **2004**, *576* (3), 363–368.
- (26) McClain, S. M.; Ojoawo, A. M.; Lin, W.; Rienstra, C. M.; Murphy, C. J. Interaction of Alpha-Synuclein and Its Mutants with Rigid Lipid Vesicle Mimics of Varying Surface Curvature. ACS Nano 2020, 14 (8), 10153–10167.
- (27) Takamori, S.; Holt, M.; Stenius, K.; Lemke, E. A.; Grønborg, M.; Riedel, D.; Urlaub, H.; Schenck, S.; Brügger, B.; Ringler, P.; *et al.* Molecular Anatomy of a Trafficking Organelle. *Cell* **2006**, *127* (4), 831–846.
- (28) Lim, L.; Wenk, M. R. Neuronal Membrane Lipids Their Role in the Synaptic Vesicle

- Cycle. In *Handbook of Neurochemistry and Molecular Neurobiology*; Tettamanti, G. and Goracci, G. Eds.; Springer LLC, Boston, MA, 2009; pp 223–238.
- (29) Bosco, D. A.; Fowler, D. M.; Zhang, Q.; Nieva, J.; Powers, E. T.; Wentworth, P.; Lerner, R. A.; Kelly, J. W. Elevated Levels of Oxidized Cholesterol Metabolites in Lewy Body Disease Brains Accelerate alpha-synuclein Fibrilization. *Nat. Chem. Biol.* 2006, 2 (5), 249–253.
- (30) Liu, J.-P.; Tang, Y.; Zhou, S.; Mclean, C.; Li, H. Cholesterol Involvement in the Pathogenesis of Neurodegenerative Diseases. *Mol. Cell. Neurosci.* **2009**, *43*, 33–42.
- (31) Man, W. K.; De Simone, A.; Barritt, J. D.; Vendruscolo, M.; Dobson, C. M.; Fusco, G. A Role of Cholesterol in Modulating the Binding of alpha-synuclein to Synaptic-Like Vesicles. *Front. Neurosci.* **2020**, *14*, 18.
- (32) Mahapatra, A.; Mandal, N.; Chattopadhyay, K. Cholesterol in Synaptic Vesicle Membranes Regulates the Vesicle-Binding, Function, and Aggregation of alphasynuclein. J. Phys. Chem. B 2021, 125 (40), 11099–11111.
- (33) Jiang, Z.; De Messieres, M.; Lee, J. C. Membrane Remodeling by alpha-synuclein and Effects on Amyloid Formation. *J. Am. Chem. Soc.* **2013**, *135* (43), 15970–15973.
- (34) Rawicz, W.; Olbrich, K. C.; McIntosh, T.; Needham, D.; Evans, E. A. Effect of Chain Length and Unsaturation on Elasticity of Lipid Bilayers. *Biophys. J.* **2000**, *79* (1), 328–339.
- (35) Mitra, K.; Ubarretxena-Belandia, I.; Taguchi, T.; Warren, G.; Engelman, D. M. Modulation of the Bilayer Thickness of Exocytic Pathway Membranes by Membrane

- Proteins Rather than Cholesterol. *Proc. Natl. Acad. Sci. U. S. A.* **2004**, *101* (12), 4083–4088.
- (36) Lapinski, M. M.; Castro-Forero, A.; Greiner, A. J.; Ofoli, R. Y.; Blanchard, G. J. Comparison of Liposomes Formed by Sonication and Extrusion: Rotational and Translational Diffusion of an Embedded Chromophore. *Langmuir* 2007, 23 (23), 11677–11683.
- (37) Karal, M. A. S.; Mokta, N. A.; Levadny, V.; Belaya, M.; Ahmed, M.; Ahamed, M. K.; Ahammed, S. Effects of Cholesterol on the Size Distribution and Bending Modulus of Lipid Vesicles. *PLoS One* **2022**, *17* (1), e0263119.
- (38) Yang, J. A.; Murphy, C. J. Evidence for Patchy Lipid Layers on Gold Nanoparticle Surfaces. *Langmuir* **2012**, *28* (12), 5404–5416.
- (39) Zhang, X.; Pandiakumar, A. K.; Hamers, R. J.; Murphy, C. J. Quantification of Lipid Corona Formation on Colloidal Nanoparticles from Lipid Vesicles. *Anal. Chem.* 2018, 90 (24), 14387–14394.
- (40) Folch, J.; Lees, M.; Sloane Stanley, G. H. A Simple Method for the Isolation and Purification of Total Lipides from Animal Tissues. *J. Biol. Chem.* **1957**, *226* (1), 497–509.
- (41) Bligh, E. G.; Dyer, W. A Rapid Method Of Total Lipid Extraction And Purification.

 Can. J. Biochem. Physiol. 1959, 37 (8), 911–917.
- (42) Rhoades, E.; Ramlall, T. F.; Webb, W. W.; Eliezer, D. Quantification of alpha-synuclein Binding to Lipid Vesicles Using Fluorescence Correlation Spectroscopy. *Biophys. J.* **2006**, *90* (12), 4692–4700.

- (43) Yang, J. A.; Johnson, B. J.; Wu, S.; Woods, W. S.; George, J. M.; Murphy, C. J. Study of Wild-Type α-Synuclein Binding and Orientation on Gold Nanoparticles. Langmuir 2013, 29 (14), 4603–4615.
- (44) Liu, J.; Bu, B.; Crowe, M.; Li, D.; Diao, J.; Ji, B. Membrane Packing Defects in Synaptic Vesicles Recruit Complexin and Synuclein. *Phys. Chem. Chem. Phys.* **2021**, *23* (3), 2117–2125.
- (45) Qi, Z.; Wan, M.; Zhang, J.; Li, Z. Influence of Cholesterol on the Membrane Binding and Conformation of alpha-synuclein. *J. Phys. Chem. B* **2023**, *127*, 1956-1964.
- (46) Papaneophytou, C. P.; Grigoroudis, A. I.; McInnes, C.; Kontopidis, G. Quantification of the Effects of Ionic Strength, Viscosity, and Hydrophobicity on Protein-Ligand Binding Affinity. *ACS Med. Chem. Lett.* **2014**, *5* (8), 931–936.
- (47) Hianik, T.; Ostatná, V.; Sonlajtnerova, M.; Grman, I. Influence of Ionic Strength, pH and Aptamer Configuration for Binding Affinity to Thrombin. *Bioelectrochemistry* 2007, 70 (1), 127–133.
- (48) Wang, X.; Zhang, S.; Xu, Y.; Zhao, X.; Guo, X. Ionic Strength-Responsive Binding between Nanoparticles and Proteins. *Langmuir* **2018**, *34*, 8264-8273.
- (49) Turner, J. G.; Murphy, C. J. How Do Proteins Associate with Nanoscale Metal-Organic Framework Surfaces? *Langmuir* **2021**, *37* (32), 9910–9919.
- (50) Rovere, M. Circular Dichroism and Isothermal Titration Calorimetry to Study the Interaction of alpha-synuclein with Membranes. *Methods Mol. Biol.* **2019**, *1948*, 123–143.
- (51) Ladokhin, A. S.; Fernández-Vidal, M.; White, S. H. CD Spectroscopy of Peptides and

- Proteins Bound to Large Unilamellar Vesicles. J. Membr. Biol. 2010, 236 (3), 247–253.
- (52) Fusco, G.; De Simone, A.; Gopinath, T.; Vostrikov, V.; Vendruscolo, M.; Dobson, C. M.; Veglia, G. Direct Observation of the Three Regions in alpha-synuclein That Determine Its Membrane-Bound Behaviour. *Nat. Commun.* 2014, 5, 3827.
- (53) Doherty, C. P. A.; Ulamec, S. M.; Maya-Martinez, R.; Good, S. C.; Makepeace, J.; Khan, G. N.; van Oosten-Hawle, P.; Radford, S. E.; Brockwell, D. J. A Short Motif in the N-Terminal Region of alpha-synuclein Is Critical for Both Aggregation and Function. *Nat. Struct. Mol. Biol.* 2020, 27 (3), 249–259.
- (54) Perrault, S. D.; Chan, W. C. W. Synthesis and Surface Modification of Highly Monodispersed, Spherical Gold Nanoparticles of 50-200 nm. *J. Am. Chem. Soc.* 2009, 131 (47), 17042–17043.
- (55) Determination of Total Phosphorus https://avantilipids.com/tech-support/analytical-procedures/determination-of-total-phosphorus (accessed Jun 3, 2023).
- (56) Kloepper, K. D.; Woods, W. S.; Winter, K. A.; George, J. M.; Rienstra, C. M. Preparation of alpha-synuclein Fibrils for Solid-State NMR: Expression, Purification, and Incubation of Wild-Type and Mutant Forms. *Protein Expr. Purif.* **2006**, *48* (1), 112–117.

For Table of Contents Only

